Growing manipulators through feeding material outside-in: Inversion robots

Xinyi Pi[1], Junke Yao[2], Benjamin Adams[3], Antonia Gerontati[4] and Helge A. Wurdemann[1]

***Abstract*— Soft eversion robots have demonstrated significant advantages in navigating within confined spaces with minimal friction, making them promising candidates for various intraluminal applications in medical, industrial, and exploratory domains. While these type of growing robots enable frictionless movement within hollow structures, no existing soft robotic actuation mechanism can grow along the outer surface of an environment without generating friction. A robot with these capabilities could open new possibilities, such as endoscopic vein harvesting for coronary artery bypass graft surgery. This paper introduces a novel growing robotic manipulator based on an outside-in material feeding mechanism - the inversion robot. Unlike conventional eversion robots, which expand by feeding material from the inside out, the inversion robot draws material from the outside to the inside, encapsulating its external environment within an inner sleeve to achieve frictionless movement. We present the design, implementation, and experimental validation of this inversion robot, investigating its growth behavior under varying pressure values and with different diameters, its ability to navigate along defined trajectories, and with a tools mounted to its tip. This inversion robot could enable vein dissection while preserving the surrounding fat layer, making it a promising innovation for minimally invasive vascular surgery and beyond.**

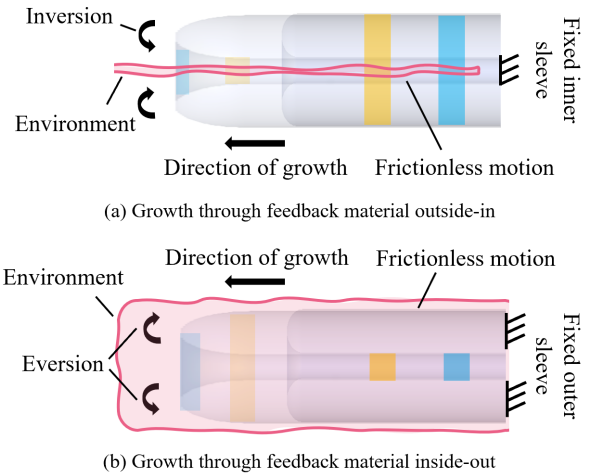

(a) Growth through feedback material outside-in

(b) Growth through feedback material inside-out

Fig. 1. Comparison of growing manipulators: The fundamental difference between (a) our new inversion robot and (b) the well-known eversion robot is that our manipulator grows by feeding material from the outside to the inside rather than feeding material from the inside to the outside, as is the case for the traditional eversion robot. Hence, our robot will introduce frictionless motion between the robot and the external environment that is encapsulated by the inner sleeve.

I. Introduction

Soft eversion robots emulate the natural growth patterns of plants, such as vines and shoots, by utilizing apical tip growth mechanisms. Their natural compliance allows them to conform to complex environments and interact delicately with surrounding objects. Additionally, by everting material at the tip from the inside to the outside to extend their structure, eversion robots exhibit a unique advantage: the growing body remains stationary relative to the environment, thereby eliminating frictional forces during navigation [1]. Due to these characteristics, eversion robots have been explored for a wide range of applications, including deployable structures [2]–[4], confined-space navigation [5]–[7], and dexterous manipulation [8]–[10]. They also hold significant promise in the medical field, with potential applications in minimally invasive procedures such as endoscopy and endovascular surgery [11]–[13].

In general, eversion robots are well-suited for exploring the internal lumen of hollow structures due to their frictionless interaction between the robot's outer layer and the surrounding environment [14]. However, to the best of the authors' knowledge, there is currently no soft robotic actuation mechanism capable of navigating along the outer surface of a tube without generating friction. Addressing this limitation could unlock novel applications, for instance, in endoscopic vessel harvesting for coronary artery bypass graft surgery [15]. One procedural step includes to harvest a vein, typically from the leg, to be used as a bypass graft. The procedure can be done minimally invasive through endoscopic vein harvesting [16]. This technique involves making small incisions (about 1-2 cm) and inserting an endoscope to guide the vein removal, using a rigid shaft and coagulation instruments to dissect and seal the vein. To reduce friction between the instrument and the surrounding environment, CO_2 is insufflated to create a working tunnel providing a thin gas layer. Once removed, the vein is cleaned, checked for damage, and prepared for grafting to restore blood flow to the heart. One challenge of endoscopic vein harvesting is to preserve the integrity of the dissected vein, as conventional

This work is supported by the Springboard Award of the Academy of Medical Sciences (grant number: SBF003-1109) and the Department of Mechanical Engineering, University College London, UK.

[1]X. Pi and H.A. Wurdemann are with the Department of Mechanical Engineering, University College London, UK, e-mail: h.wurdemann@ucl.ac.uk

[2]J. Yao is with the Department of Engineering, King's College London and Department of Mechanical Engineering, University College London, UK.

[3]B. Adams is with the Barts Heart Centre, St. Bartholomew's Hospital and with the Institute of Cardiovascular Medicine, University College London, UK.

[4]A. Gerontati is with the Chelsea and Westminster NHS Trust and the Centre for Perioperative Medicine Division of Surgery & Interventional Sciences, University College London, UK.

techniques might cause damage due to the rigid nature of current surgical tools [17]. Moreover, existing methods do not allow for simultaneous harvesting of the surrounding fat layer, which has been shown to provide protective benefits for the graft [18]. A frictionless, soft robotic tool designed for this task could maintain the surrounding fat layer, potentially improving graft quality and long-term surgical outcomes.

The contribution of this paper lies in a new concept for growing robotic manipulators through outside-in material feeding - the inversion robot, see Fig. 1(a). Unlike conventional eversion robots as shown in Fig. 1(b), which expand by feeding material from the inside out, our approach enables growth by drawing material from the outside to the inside. Hence, the inversion robot's unique outside-in material feeding mechanism enables frictionless motion between any external environment, that is encapsulated by the inner sleeve. In addition, soft and flexible materials, commonly used in eversion robots, possess inherent compliance that allow them to conform the shape of the surrounding soft tissue. We present the design, implementation, and experimental evaluation of this new inversion robot. We believe that a potential application of this new inversion robot concept is endoscopic vein harvesting. The frictionless, soft robotic mechanism could enable dissection of a vein, while also preserving the surrounding fat layer.

In Section II, we introduce the overall concept of the inversion robot, in particular, its material storage method and the actuation principle. Then, Section III details the design and the manufacturing process. The experimental evaluation is included in Section IV, reporting on the setup, protocol, and results. The experiments investigate the manipulator's growth under various pressure values and for different diameters, along defined trajectories and with a tool at its tip. Finally, we discuss limitations and future directions for our new concept of a growing robot in Section V.

II. Concept of the Inversion Robot: Feeding Material from the Outside to the Inside

The concept comparison of the eversion robot and the inversion robot is illustrated in Fig. 1. For the well-known eversion robot, the outer sleeve is typically anchored to the base port, while the inner sleeve or tail is stored by reeling around a central shaft [19]. The robot extends by applying internal pressure while fixing the outer layer and releasing the inner sleeve or tail, which is stored in a spool (see Fig. 1(b)). Instead, the concept of our inversion robot in Fig. 1(a) achieves growth by an inverse mechanism-releasing the outer layer while fixing the inner tail - also utilizing pressure actuation. This difference in concept results in the design of a new operational mechanism, allowing to apply pressure within the inner and outer sleeve and, at the same time, feeding material of the sleeve from the outside.

The feeding mechanism for the inversion robot is illustrated in Fig. 2. In the initial state (Fig. 2(a)), the inner sleeve (or tail) is secured to the base by a tensile force generated through an internal tendon, ensuring that the inner layer remains stationary while maintaining an airtight seal.

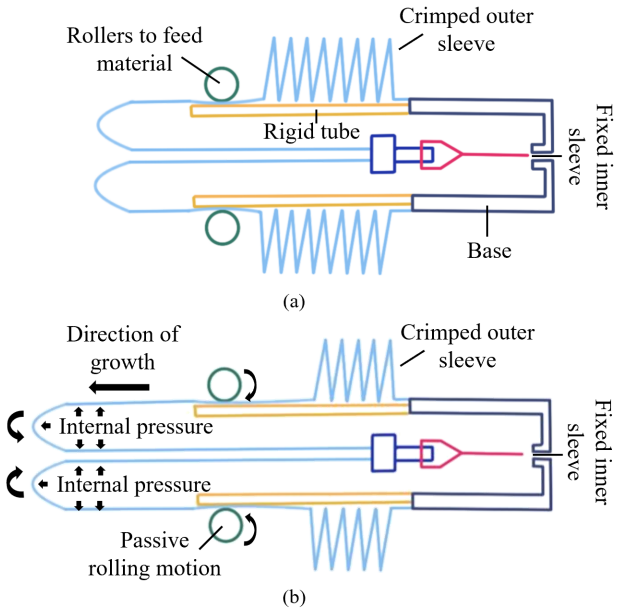

Fig. 2. Concept and mechanism of the inversion robot: (a) In the initial state, the inner sleeve is fixed and mounted to the base. The outer sleeve is crimped along a supporting structure made of a rigid tube. (b) Once internal pressure is applied, the resulting forces on the inner sleeve result in a material intake from the crimped outer sleeve. A consistent feeding of material is facilitated by passively rotating rollers, which guide the sleeve smoothly as it advances between the rigid tube and the roller system, ensuring seamless progression.

Meanwhile, the outer sleeve is crimped along a supporting structure composed of a rigid tube. Passively rotating rollers prevent the crimped sleeve from dislodging from the rigid tube, when no pressure is applied. This design preserves internal pressurization without compromising the tube's structural integrity, while also minimizing the stored material length. In addition, crimping the outer layer near the tube's open end enhances system sealing, ensuring that the structure remains securely attached to the base port. In fact, similar crimping techniques have been employed in certain eversion robot designs to sustain a functional central working channel [20]–[22].

Under pneumatic air actuation, the internal pressure generates forces at the robot's tip, as illustrated in Fig. 2(b). With the inner tail immobilized by a tendon connected to the base and the outer layer advancing by overcoming friction at the crimped sleeve - a process facilitated by passively rotating rollers - the material undergoes a controlled inversion transition as the robot extends and grows. This mechanism enables continuous elongation of the robot body while preserving a fixed relative position between the inner sleeve and the central working channel, thereby implementing the inverted growth strategy.

III. Design of the Inversion Robot Prototype

The design of the proposed inversion robot in Fig. 3 introduces a technique that enables continuous growth through feeding additional material of the sleeve from the outside to the inside. The system consists of an externally pressurized

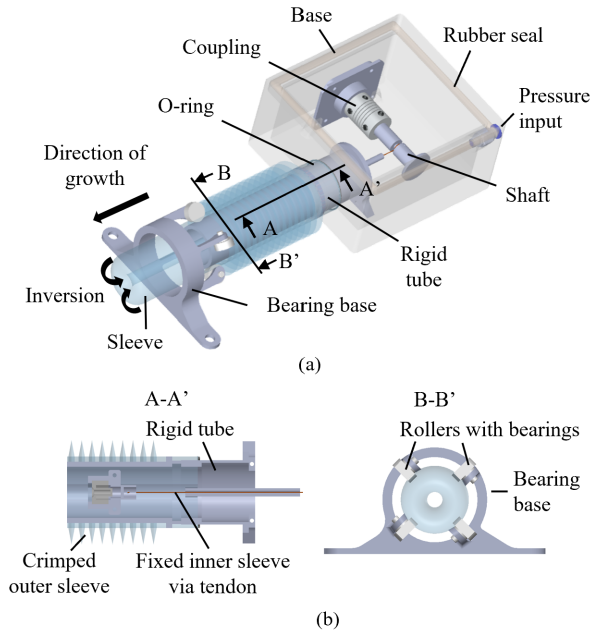

Fig. 3. (a) Overview of the prototype, showing the base, which houses the mounted coupling and shaft, to which the inner sleeve is connected via a tendon. The base is sealed with rubber to maintain positive pressure when actuated through the pressure input. The rigid tube, where the outer sleeve is crimped, serves as the connection point for the inversion robot. (b) Cross-sectional views of the inversion robot and its tip, illustrating the rollers guiding the crimped outer sleeve under pressurization. The inner sleeve remains fixed to the tendon, while the outer sleeve is securely crimped along the rigid tube, ensuring controlled material feeding and continuous robot extension.

base, the robot's sleeve, that is crimped along a rigid tube on the outside at the one end and connected to the base via a tendon on the inside at the other end. A passive roller, mounted to a bearing base, supports the consistent feeding of material during the growth phase.

A. Growing the manipulator through the outer sleeve

To enable inversion-based growth, a system was developed comprising a base with a pressure inlet for air pressure regulation and the robot sleeve, as illustrated in Fig. 3(a). The internal pressure of the base is controlled using a Camozzi K8P proportional pressure regulator (Camozzi Automation Ltd. Warwickshire, UK), utilizing the pneumatic control platform developed by Shi et al. [23].

The robot body's sleeve is constructed using narrow LayFlat tubing (LFT), with one end securely sealed to the port over the rigid tube via an O-ring to ensure airtightness. The material is radially crimped along the rigid tube, to guide and feed additional material of the outer sleeve, as shown in Fig. 3(b) (left). At the distal end of the rigid tube, four rollers with bearings are positioned to maintain full contact with both the outer sleeve and the rigid tube. These roller with bearings are supported by a bearing base and are designed to allow the outer sleeve to slide out smoothly while keeping the shaft of the roller stationary, ensuring controlled material feeding during growth (see Fig. 3(b) - right). To enhance interaction between the roller with bearing and the robot sleeve, the contact surface of the roller is coated with Smooth-Sil 960 (Smooth-On, Inc. PA, United States) silicone material using injection molding. This high-friction coating generates sufficient grip between the roller and the sleeve material, ensuring reliable material feeding during growing.

The inner sleeve is sealed by a heat sealer to ensure airtightness and then connected to a tendon, made from Ultra High Molecular Weight Polyethylene Dyneema. The tendon, tightly connected to the inner sleeve, is routed through a central pipe within the robot's body. This centralized tendon alignment prevents unintended lateral forces, thereby improving directional stability during deployment. At the base of the system, a shaft is coupled to the base and firmly mounted using 3D-printed structural supports by material Tough 2000 (Formlabs, Somerville, Massachusetts, United States). The tendon is fixed to the shaft. The top of the base is sealed with rubber, and airflow is regulated via a one-way air valve, which provides the necessary internal pressure for robot actuation and growth.

B. Design and manufacturing of the sleeve

We manufactured a robot sleeve with a 25 mm and 33 mm diameter and a wall thickness of 120 gauge. This specific thickness was selected to minimize friction between the crimped outer layers, ensuring smooth deployment. The diameter of the rigid tube is set to 22 mm and 30 mm, respectively, which is slightly smaller than the robot sleeve's diameters. This dimension optimally balances material storage capacity and structural support. If the gap between the sleeve and the rigid tube is too large, the inflated sleeve could be squeezed by the rollers, and could not act in smooth sliding motion. The rigid tube has a length of 90 mm, allowing it to accommodate 250 mm of crimped material.

IV. Experimental Setup, Protocol, Results and Discussion

A. Experimental Setup

The experimental setups are shown in Fig. 4. In all experiments, growth lengths were recorded using a ruler at various growing stages. The internal pressure was precisely controlled using the Camozzi K8P proportional pressure regulator, which regulated airflow. To measure the tensile force exerted by the tendon, an IIT-FT17 6 DoF force/torque sensor was attached to the tendon, that connects the inner sleeve of the robot to the base. In addition, the growth duration was automatically logged within the control platform, ensuring accurate time measurements for deployment analysis. This setup, as shown in Fig. 4(a) was used for Experiment 1 and 2. For Experiment 3 and 4, a soft and rigid phantom of a vessel with diameters of 6 mm and 8 mm, respectively, was added, so that the robot could grow along this environment. The soft phantom was made of silicone material, whereas the rigid phantom was made of polylactic acid (PLA) material. In Experiment 4, a magnetic cap was mounted onto the robot's tip, to support growth during free elongation.

B. Experimental Protocol and Results

Four experiments have been conducted following a number of systematic steps:

1) The sleeve of the robot was cut to a length of approximately 65 cm, corresponding to a target growth length of 25 cm. One end of the sleeve was sealed using a heat sealer to form a closed tube. The inner sleeve was attached to a tendon, which was then mounted on the force/torque sensor, measuring the tendon forces during deployment.
2) The outer sleeve was crimped along the rigid tube. The rollers were connected to the end of the tube, maintaining a layer of the outer sleeve between the tube and rollers. The sleeve was then everted and the inner sleeve connected to the tendon. The robot's tip was positioned at the initial position.
3) The rubber-sealed robot base was connected to the pneumatic platform, which supplied pressure values for a predetermined period to drive the robot's growth. A camera system recorded the robot's displacement, while the force sensor captured the tendon force variations throughout the growth process.
4) After each trial, the robot base was disconnected from the pressure supply, and the system was manually reset to its initial state. This was achieved by crimping the extended sleeve back along the rigid tube, restoring the configuration for the next experiment/trial.
5) After completing a set of trials for one of the four experiments, the tube was removed from the base. A new tube was stored for the next experiment.

For each of the four experiments, ten trials were conducted. The recorded data, including tendon force variation over time and pressure readings, were imported into MATLAB for further analysis. The tendon force reflects the internal mechanical interaction between the fixed inner sleeve and the actuated outer sleeve during growth, serving as an indicator of internal tension and resistance within the system. In addition, recordings from the top-mounted camera returned growth data and time.

1) Experiment 1 – Growth at different pressure values: This experiment aimed to evaluate the influence of different air pressures on the growth process and the corresponding force exerted on the tendon. The inversion robot, with a diameter of 33 mm, was actuated 10 times under three pressure levels: 0.15, 0.2, and 0.3 bar. In each trial, the robot was grown to a length of 25 cm, while the tendon force was continuously recorded throughout the process.

Results: Fig. 5 illustrates the time required for the robot to extend to 25 cm under different pressure levels: 0.15, 0.2, and 0.3 bar, represented by the dashed orange, rigid purple, and dotted green lines, respectively. Simultaneously, the tendon forces were recorded throughout the growing phase. Each condition was tested 10 times, and the averaged values are presented. The black dots indicate the moment when the tendon force drops, marking the completion of the growth process. For a pressure of 0.15 bar, the robot required approximately 10.5 seconds to reach the target length, with a standard deviation (SD) of 1.1 seconds. At 0.2 bar, the duration decreased to 9.0 seconds (SD of time: 1.8 seconds), while at 0.3 bar, the recorded time was 5.6 seconds (SD of time: 1.4 seconds). These results confirm that higher pressure leads to faster robot extension. During the growing phase, the tendon force initially exhibits fluctuations before gradually increasing and reaching a peak. After stabilizing for a short period, the force then gradually decreases as the robot completes its extension.

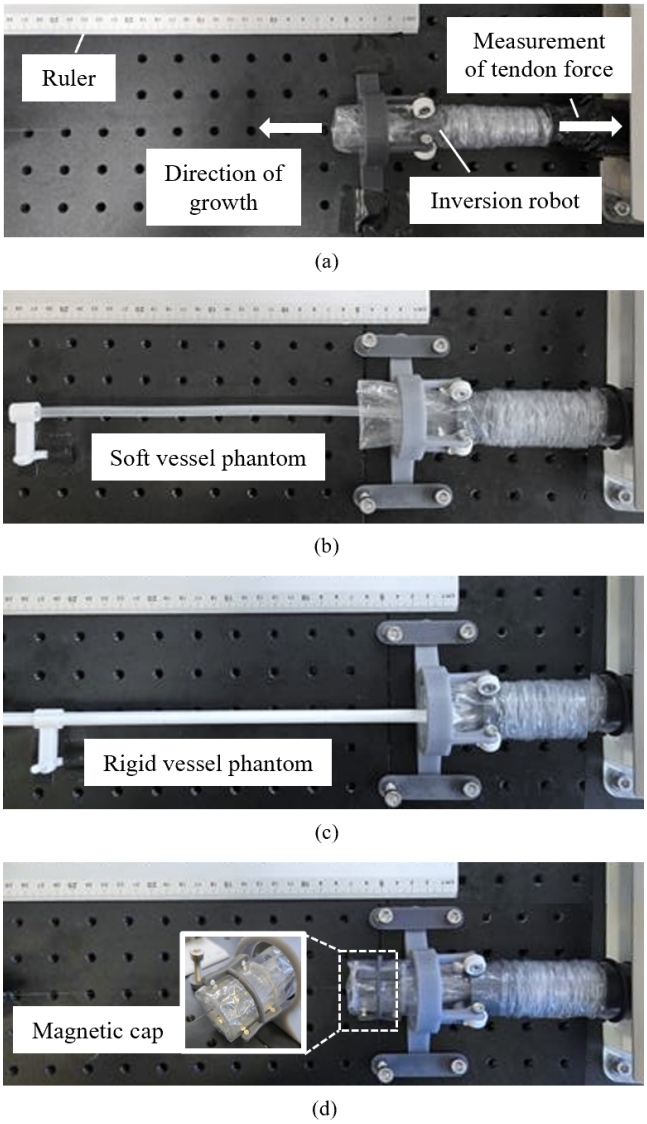

Fig. 4. Experimental setup: (a) Experiment 1 and 2: The inversion robot (made of a 33 mm and 25 mm diameter for Experiment 1 and 2, respectively) is actuated with a range of pressure values. Force measurements are recorded acting on the tendon that connects the inner sleeve to the base. A ruler is used to measure the tip location while growing. At the same time, the inner pressure variation is monitored. (b) and (c) Experiment 3: The inversion robot with a 33 mm diameter and 25 cm length grows along a soft and rigid phantom of a vessel. The soft phantom was made of silicone material, whereas the rigid phantom was made of polylactic acid material. (d) Experiment 4: A magnetic cap is mounted onto the robot's tip, to support growth during free elongation. Tendon forces are compared to Experiment 1.

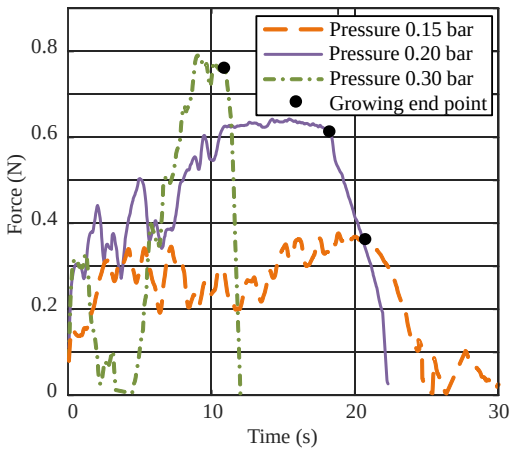

Fig. 5. Results for Experiment 1: Force recordings over time, when the robot is actuated with 0.15, 0.2 and 0.3 bar air pressure, reaching a total growing length of 25 cm (indicated by the black dot). The larger the pressure and forces on the tendon, the shorter the time required to grow.

2) Experiment 2 – Understanding growing behavior of robots with different diameters: Inversion robots with a 33 mm and 25 mm diameter and length of 25 cm were tested. Under a constant pressure of 0.2 bar, the tendon forces were recorded throughout the growth process.

Results: Fig. 6 presents the growth time and tendon force measurements for two robots with diameters of 33 mm and 25 mm, respectively, as they extend to 25 cm under a constant pressure of 0.2 bar. The force trend for the 33 mm robot is represented by the solid purple line, while the 25 mm robot is indicated by the dashed red line. Each experiment was repeated 10 times, and the averaged results are shown. The robot at 25 mm diameter at 0.2 bar required approximately 18.1 seconds to reach the target length (SD of time: 0.6 seconds). A sudden drop in force without subsequent recovery marks the completion of the growth process. The maximum force observed for both diameters is approximately 0.6 N. Thus, the 25 mm robot requires a longer duration to complete growth and exhibits greater force fluctuations throughout the process.

3) Experiment 3 – Unconstrained growing versus growing along phantom environments: To evaluate the ability of the inversion robot to grow along predefined trajectories and encapsulate an environment, two types of vessel phantoms were prepared: a rigid and a soft phantom. For the rigid phantom, the robot grew along a PLA phantom. Similarly, a silicone phantom was used to simulate a soft vessel. The robot was actuated at a constant pressure of 0.2 bar, growing to a length of 25 cm. In both cases, the tendon force was recorded throughout the growth process.

Results: Fig. 7 presents the time required for a 33 mm diameter robot to grow 25 cm along different phantom environments: a soft (dashed blue) and a rigid phantom vessel (dotted pink). The robot was actuated at a constant pressure of 0.2 bar. The robot along the soft phantom vessel required approximately 7.3 seconds to reach the target length (SD: 0.9 seconds), while the rigid phantom required 6.7 seconds with an SD of 1.0 seconds. The tendon forces were recorded throughout the growth process. The force drop indicates the completion of growth, with the rigid phantom requiring the shortest time. The maximum tendon forces recorded varied across environments: For the unconstrained growth, the force peaked at approximately 0.6 N, while for the phantoms, the forces were around 0.4 N and 0.2 N, respectively. For the rigid phantom, the force reached its peak value before exhibiting significant fluctuations.

4) Experiment 4 – Robot behavior with a tool mounted on tip: Carrying a tool at the tip is an important requirement for a medical instrument, which is investigated by this experiment. A cap with a magnet was selected due to its secure attachment and minimal risk of damaging the robot body, as shown in Fig. 4(d), which provides a zoomed-in view of the cap. The growing pressure was set to 0.15 bar, and the robot reached a length of 25 cm.

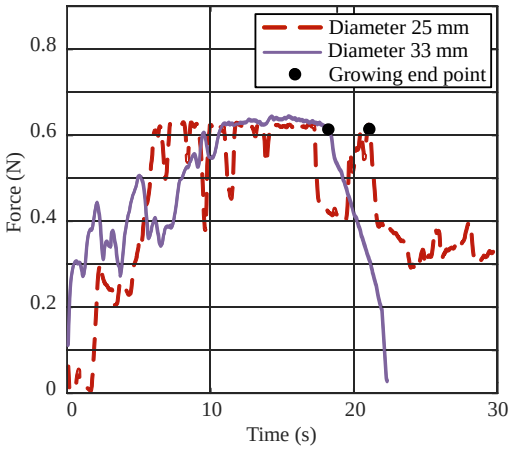

Fig. 6. Results for Experiment 2: Force recordings over time when robots with a diameter of 25 mm and 33 mm were pressurized by 0.2 bar. The time to reach 25 cm was recorded. The smaller diameter robot takes longer to grow, whereas the tendon forces are of similar average values.

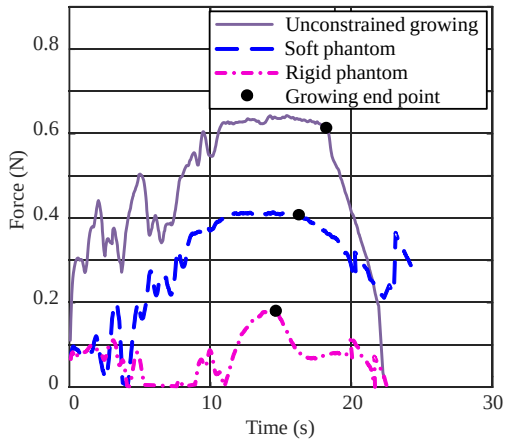

Fig. 7. Results for Experiment 3: Force measurements over time for the robot, when growing in an unconstrained way and when growing along a soft and rigid phantom of a vessel. The stiffer the path, the smaller the tendon force required and the faster the growth rate.

Results: Fig. 8 presents the difference in growth time and force with and without a tip-mounted tool. The experiment was conducted using a robot with a diameter of 33 mm and a growth length of 25 cm while maintaining a constant growing pressure of 0.15 bar. The robot with a magnetic cap required approximately 9.1 seconds to reach the target length (SD: 0.3 seconds). The force measurements of the robot without a tip tool are represented by the dashed orange line, and the force measurements of the robot with a tip tool are represented by the gold line. The results show that the tendon force required for the robot with a tip tool is greater than that of the robot without a tip tool. The force fluctuations are more pronounced when the tool is attached, especially in the middle stage of the growth process.

C. Discussions

The experimental results provide insights into the growth behavior, stability, and functional capabilities of the inversion robot. By systematically analyzing the effects of pressure, diameter, trajectory following, and tool attachment, a better understanding of the fundamental factors influencing the robot's performance was achieved. These findings contribute to optimizing control strategies and enhancing the robot's adaptability for real-world applications.

For the experiment of the robot growing at different pressure values, the results demonstrate that the robot achieves faster growth when higher pressure values are applied, which validates an expected behavior as observed in eversion robots: Internal pressure serves as the primary driving force for growth. As the air pressure increases, a greater expansion force is generated, reducing the time required for the robot to reach a fixed length. Consequently, robots of the same diameter exhibit higher growth speeds under higher pressures. Simultaneously, the tendon force is responsible for maintaining system equilibrium, and its magnitude increases with the increase in applied pressure and resistance in the material feeding process. 0.15 bar is the minimum air pressure that can make a robot growth with a diameter of 33 mm. Below this threshold, friction between the crimped sleeve significantly hinders the growing process, leading to an uneven and inconsistent growth pattern.

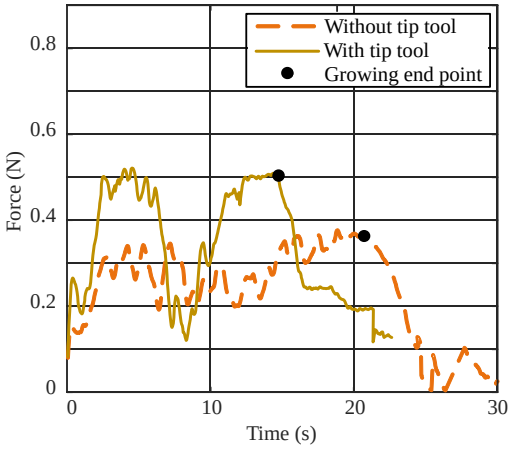

Fig. 8. Results for Experiment 4: Force recordings over time for a robot with and without a tool mounted at the tip, reaching a growing length of 25 cm. The increase in tendon force after adding the tip tool is because the robot needs to overcome the friction generated by the tip. A sudden decrease in force is caused by the tool being stuck during the growth process.

In addition, variations in force fluctuations indicating instability are observed across different pressure levels, while a continuous drop signals the completion of the growth process, as there is no active tension. At higher pressures, force fluctuations are reduced, while at lower pressures, the frequency of oscillations increases. This may be attributed to the fact that at elevated pressures, the resistance from the crimped sleeve is quickly overcome, allowing the system to stabilize more rapidly. In contrast, at lower pressures, each layer of the crimped sleeve takes longer to slide, causing more fluctuations in the force. Compared to conventional eversion robots that employ the crimping method [22], the tendon force in the inversion robot are significantly lower, highlighting its efficiency.

The effect of diameter on growth performance reveals that tendon force is relatively independent of diameter variations. However, robots with smaller diameters require longer growth times and exhibit higher force fluctuation frequencies. This is likely due to the resistance of the crimped sleeve is higher. Under the same crimping conditions (where the length of the rigid tube remains constant), the gap between the crimped sleeve of small diameter is compressed smaller and tighter, leading to reduced system stability and slower growth. In the case of a 25 mm diameter robot, a sudden drop was caused by the robot getting stuck. Despite this challenge, the results confirm the feasibility of miniaturizing the inversion robot by controlling the diameter of the robot body and the size of its components.

The experiment on encapsulating a phantom vessel shows that following a predefined environment reduces tendon force. Also, higher stiffness contributes to faster growth and quicker stabilization of system oscillations. This is because a guided path provides structural support to the robot tip, stabilizing the tendon force magnitude and direction.

The evaluation of tool-carrying capability in Experiment 4 demonstrates that robots equipped with a tip-mounted tool require greater tendon force than those without, given the same growth pressure. This is due to the additional resistance introduced by the tool, which the robot must overcome. However, the presence of a tool also facilitates smoother growth, as reflected in the increased growth speed and reduced fluctuations. This finding confirms that the inversion robot is capable of carrying a tip-mounted tool, similar to conventional eversion robots [24]–[26].

While our inversion robot demonstrates stable growth and the ability to carry a tool, certain limitations require further exploration. At lower pressures, force fluctuations can affect growth stability, highlighting the need for adaptive pressure control. In addition, miniaturization may introduce challenges related to crimped storage, and overall stability, which could be addressed through optimized storage configurations and active material feeding with bearing control. Future work

will also focus on enhancing end-effector integration to improve functionality. Addressing these aspects will contribute to refining the robot's design and expanding its applications.

V. CONCLUSIONS AND FUTURE WORK

This work presented a new approach to growing and eversion robots through an outside-in material feeding mechanism, introducing the inversion robot as a novel alternative to conventional eversion-based systems. By drawing material inward, this design achieves frictionless motion between the robot's sleeve and an encapsulated environment. Through detailed experimental validation, we have demonstrated that the robot's growth behavior is influenced by key factors, including internal pressure, diameter, trajectory constraints, and tip-mounted tools. Higher pressure values resulted in faster deployment, while environmental constraints and tool attachment affected tendon force requirements and overall stability. Our robot could unlock new possibilities for applications in the medical domain. In particular, its potential to enable vein dissection while preserving the surrounding fat layer highlights its transformative role in vascular interventions such as endoscopic vein harvesting. Our work allows further advancements in soft robotic manipulators, offering a new technique for frictionless growth mechanisms.

Future work will focus on enhancing the robot's robustness and adaptability in complex environments. Key areas include optimizing materials for durability, growth length and tissue compatibility, potentially incorporating bio-compatible lubricating fluids or membrane-infused channels to reduce friction and create a protective interface with surrounding biological tissue. Additional efforts will develop active bearing control by managing roller-induced friction for stable material feeding, miniaturizing the robot, and designing an effective retraction mechanism.

REFERENCES

[1] L. H. Blumenschein, M. M. Coad, D. A. Haggerty, A. M. Okamura, and E. W. Hawkes, "Design, modeling, control, and application of everting vine robots," *Front. Robot. AI*, vol. 7, p. 548266, 2020.

[2] N. Agharese, T. Cloyd, L. H. Blumenschein, M. Raitor, E. W. Hawkes, H. Culbertson, and A. M. Okamura, "Hapwrap: Soft growing wearable haptic device," *IEEE Int. Conf. Robot. Autom.*, pp. 5466–5472, 2018.

[3] M. Raitor, J. M. Walker, A. M. Okamura, and H. Culbertson, "Wrap: Wearable, restricted-aperture pneumatics for haptic guidance," *IEEE Int. Conf. Robot. Autom.*, pp. 427–432, 2017.

[4] L. T. Gan, L. H. Blumenschein, Z. Huang, A. M. Okamura, E. W. Hawkes, and J. A. Fan, "3d electromagnetic reconfiguration enabled by soft continuum robots," *IEEE Robotics and Automation Letters*, vol. 5, no. 2, pp. 1704–1711, 2020.

[5] M. M. Coad, R. P. Thomasson, L. H. Blumenschein, N. S. Usevitch, E. W. Hawkes, and A. M. Okamura, "Retraction of soft growing robots without buckling," *IEEE Robotics and Automation Letters*, vol. 5, no. 2, pp. 2115–2122, 2020.

[6] P. Berthet-Rayne, S. H. Sadati, G. Petrou, N. Patel, S. Giannarou, D. R. Leff, and C. Bergeles, "Mammobot: A miniature steerable soft growing robot for early breast cancer detection," *IEEE Robotics and Automation Letters*, vol. 6, no. 3, pp. 5056–5063, 2021.

[7] J. Luong, P. Glick, A. Ong, M. S. DeVries, S. Sandin, E. W. Hawkes, and M. T. Tolley, "Eversion and retraction of a soft robot towards the exploration of coral reefs," *IEEE International Conference on Soft Robotics*, pp. 801–807, 2019.

[8] E. W. Hawkes, L. H. Blumenschein, J. D. Greer, and A. M. Okamura, "A soft robot that navigates its environment through growth," *Science Robotics*, vol. 2, no. 8, p. eaan3028, 2017.

[9] J. D. Greer, T. K. Morimoto, A. M. Okamura, and E. W. Hawkes, "Series pneumatic artificial muscles (spams) and application to a soft continuum robot," *IEEE Int. Conf. Robot. Autom.*, pp. 5503–5510, 2017.

[10] F. Stroppa, M. Luo, K. Yoshida, M. M. Coad, L. H. Blumenschein, and A. M. Okamura, "Human interface for teleoperated object manipulation with a soft growing robot," *IEEE International Conference on Robotics and Automation*, pp. 726–732, 2020.

[11] X. Pi, I. A. Szczech, and L. Cao, "A retractable soft growing robot with a flexible backbone," *IEEE/RSJ Int. Conf. Intell. Robots Syst.*, pp. 2477–2484, 2023.

[12] J. Davy, N. Greenidge, S. Kim, L. J. Tinsley, P. Lloyd, J. H. Chandler, R. A. Harris, T. K. Morimoto, and P. Valdastri, "Vine robots with magnetic skin for surgical navigations," *IEEE Robotics and Automation Letters*, vol. 9, no. 8, pp. 6888–6895, 2024.

[13] M. Li, R. Obregon, J. J. Heit, A. Norbash, E. W. Hawkes, and T. K. Morimoto, "Vine catheter for endovascular surgery," *IEEE Trans. Med. Robot. Bionics.*, vol. 3, no. 2, pp. 384–391, 2021.

[14] P. A. der Maur, B. Djambazi, Y. Haberthür, P. Hörmann, A. Kübler, M. Lustenberger, S. Sigrist, O. Vigen, J. Förster, F. Achermann *et al.*, "Roboa: Construction and evaluation of a steerable vine robot for search and rescue applications," *IEEE International Conference on Soft Robotics*, pp. 15–20, 2021.

[15] R. D. Lopes, G. E. Hafley, K. B. Allen, T. B. Ferguson, E. D. Peterson, R. A. Harrington, R. H. Mehta, C. M. Gibson, M. J. Mack, N. T. Kouchoukos *et al.*, "Endoscopic versus open vein-graft harvesting in coronary-artery bypass surgery," *New England Journal of Medicine*, vol. 361, no. 3, pp. 235–244, 2009.

[16] M. A. Zenati, D. L. Bhatt, F. G. Bakaeen, E. M. Stock, K. Biswas, J. M. Gaziano, R. F. Kelly, E. E. Tseng, J. Bitondo, J. A. Quin *et al.*, "Randomized trial of endoscopic or open vein-graft harvesting for coronary-artery bypass," *New England Journal of Medicine*, vol. 380, no. 2, pp. 132–141, 2019.

[17] R. E. Harskamp, R. D. Lopes, C. E. Baisden, R. J. De Winter, and J. H. Alexander, "Saphenous vein graft failure after coronary artery bypass surgery: pathophysiology, management, and future directions," *Annals of Surgery*, vol. 257, no. 5, pp. 824–833, 2013.

[18] T. Saito, H. Kurazumi, R. Suzuki, K. Matsunaga, S. Tsubone, B. Lv, S. Kobayashi, T. Nagase, T. Mizoguchi, M. Samura *et al.*, "Perivascular adipose tissue is a major source of nitric oxide in saphenous vein grafts harvested via the no-touch technique," *Journal of the American Heart Association*, vol. 11, no. 3, p. e020637, 2022.

[19] H. J. H. Kim, H. Abdel-Raziq, X. Liu, A. Y. Siskovic, S. Patil, K. H. Petersen, and H.-L. Kao, "Robotic barrier construction through weaved, inflatable tubes," *IEEE/RSJ International Conference on Intelligent Robots and Systems*, pp. 8318–8323, 2023.

[20] N. G. Kim, N. J. Greenidge, J. Davy, S. Park, J. H. Chandler, J.-H. Ryu, and P. Valdastri, "External steering of vine robots via magnetic actuation," *Soft Robotics*, 2024.

[21] C. Girerd, A. Alvarez, E. W. Hawkes, and T. K. Morimoto, "Material scrunching enables working channels in miniaturized vine-inspired robots," *IEEE Transactions on Robotics*, vol. 40, pp. 2166–2180, 2024.

[22] J.-H. Kim, J. Jang, S.-M. Lee, S.-G. Jeong, Y.-J. Kim, and J.-H. Ryu, "Origami-inspired new material feeding mechanism for soft growing robots to keep the camera stay at the tip by securing its path," *IEEE Robotics and Automation Letters*, vol. 6, no. 3, pp. 4592–4599, 2021.

[23] J. Shi, W. Gaozhang, H. Jin, G. Shi, and H. A. Wurdemann, "Characterisation and control platform for pneumatically driven soft robots: Design and applications," *IEEE International Conference on Soft Robotics*, pp. 1–8, 2023.

[24] R. Dorosh, J. Allen, Z. He, C. Ninatanta, J. Coleman, J. Spieker, E. Tuck, J. Kurtz, Q. Zhang, M. D. Whiting *et al.*, "Design, modeling, and control of a low-cost and rapid response soft-growing manipulator for orchard operations," *IEEE/RSJ International Conference on Intelligent Robots and Systems*, pp. 4184–4190, 2023.

[25] S.-G. Jeong, M. M. Coad, L. H. Blumenschein, M. Luo, U. Mehmood, J. H. Kim, A. M. Okamura, and J.-H. Ryu, "A tip mount for transporting sensors and tools using soft growing robots," *IEEE/RSJ Int. Conf. Intell. Robots Syst.*, pp. 8781–8788, 2020.

[26] M. M. Coad, L. H. Blumenschein, S. Cutler, J. A. R. Zepeda, N. D. Naclerio, H. El-Hussieny, U. Mehmood, J.-H. Ryu, E. W. Hawkes, and A. M. Okamura, "Vine robots," *IEEE Robotics & Automation Magazine*, vol. 27, no. 3, pp. 120–132, 2019.